

# Orbital Decay in LMC X-4

Alan M. Levine, Saul A. Rappaport, & Goce Zojcheski

*Department of Physics and Center for Space Research, Massachusetts Institute of Technology, Cambridge, MA 02139; aml@space.mit.edu*

## ABSTRACT

We report on the results of observations of the binary X-ray pulsar LMC X-4 with the *Rossi X-ray Timing Explorer*. Our analysis of the Doppler delays of the 13.5-s X-ray pulsations yields the most accurate determination of the LMC X-4 orbital parameters available to date. The epoch of orbital phase zero for the 1.4 day orbit is determined with an uncertainty of  $\sim 20$  s, and is combined with 5 earlier determinations of the epoch of phase zero to obtain the rate of change in the orbital period:  $\dot{P}_{orb}/P_{orb} = (-9.8 \pm 0.7) \times 10^{-7}$  yr $^{-1}$ . This is the first high significance measurement of the rate of change of the orbital period in LMC X-4.

We present data on one of three strong X-ray flares as well as energy-dependent pulse profiles for both non-flaring and flaring time intervals. The pulse profiles during the non-flaring time intervals are typically strikingly different from the flare profiles, but at other times can be similar.

We reconsider the orbital decay of LMC X-4 in the context of tidal evolution. We find that, while the orbital decay is most likely driven by tidal interactions, the asynchronism between the orbit and the rotation of the companion star is probably maintained by the evolutionary expansion of the companion star, just as is thought to be the case for Cen X-3 and SMC X-1. For LMC X-4, we find that the evidence favors the companion star being in a late stage of its life on the main sequence.

Overall, we have found in this work as well as in previous studies that the orbital decay timescales for SMC X-1, Cen X-3, and LMC X-4 are 300,000, 550,000, and 1,000,000 years, respectively. In each case, the Roche lobe will move catastrophically deep into the atmosphere within about  $10^4$  years. This short X-ray lifetime may be typical of all massive X-ray binaries in Roche-lobe or near Roche-lobe contact.

*Subject headings:* Stars:individual(LMC X-4) — stars:neutron — X-rays:stars

## 1. Introduction

The history of the orbital period of a binary star system can tell much about the physics of the stellar components and their mutual interactions. In most binaries, the evolution of the orbital period is too slow to be detectable, but there are systems in which this evolution can be measured. Among X-ray binaries, this evolution is rather apparent in a number of cases. Such binaries include Her X-1, which has an intermediate mass companion to the compact star, and Cyg X-3, which has a companion whose mass is not well determined, although it may be a high mass Wolf-Rayet star (Deeter et al. 1991, Kitamoto et al. 1995; van Kerkwijk et al. 1996 and references therein). However, it is in systems such as Cen X-3 and SMC X-1, which comprise X-ray pulsars orbiting around high mass companions, where extraordinary sensitivity to orbital changes and short orbital evolutionary timescales combine to allow orbital period changes to be measured with high precision.

Indeed, highly significant detections of orbital period changes have been made in Cen X-3 and SMC X-1. Kelley et al. (1983b) determined that the orbital period of Cen X-3 is changing at a rate  $\dot{P}_{orb}/P_{orb} = (-1.8 \pm 0.08) \times 10^{-6} \text{ yr}^{-1}$ , while Levine et al. (1993) established that  $\dot{P}_{orb}/P_{orb} = (-3.36 \pm 0.02) \times 10^{-6} \text{ yr}^{-1}$  for SMC X-1. Attempts to measure  $P_{orb}/\dot{P}_{orb}$  for LMC X-4 and 4U 1538-52 have resulted in only marginal detections or upper limits (see discussion in Woo et al. 1996; Safi-Harb, Ögelman, & Dennerl 1996, Corbet, Woo, & Nagase 1993).

Levine et al. (1993) concluded that the rapidly decreasing orbital period in SMC X-1 was most likely caused by tidal interactions between the neutron star and its massive companion. Tidal evolution requires asynchronism between the orbital motion and the rotation of the companion star. The nuclear evolution of the companion in its hydrogen shell burning phase drives rapid expansion of the star and hence a rapid increase in the stellar moment of inertia. Levine et al. (1993) argued that this results in a decrease in the rate of rotation of the companion star so that it would be rotating more slowly than required for synchronism with the orbital motion, and would set the conditions for orbital decay by tidal torques. The Darwin instability was not needed to explain the orbital decay. The inference that hydrogen burning is taking place in a shell within Sk 160, the companion to SMC X-1, was reinforced by evidence that its ra-

dius is likely to be larger than that of a main-sequence star of mass within the range of estimates for Sk 160.

Tidal interactions most likely also drive the orbital decay of Cen X-3 (Kelley 1986, Levine et al. 1993). However, Levine et al. (1993) noted that the  $12 \pm 2 \text{ R}_\odot$  radius of the companion star in this system is smaller than the  $17 \pm 1 \text{ R}_\odot$  radius of Sk 160, even though both stars have similar masses, and that this smaller radius was more likely to be consistent with the radius of a  $\sim 20 \text{ M}_\odot$  star late in its core hydrogen-burning phase. Other differences between the SMC X-1 and Cen X-3 systems were also noted, which generally made it difficult to reach firm conclusions about the exact evolutionary state of the Cen X-3 system.

Woo et al. (1996) noted that their estimate for the orbital period derivative of LMC X-4, i.e.,  $\dot{P}_{orb}/P_{orb} = (-5.3 \pm 2.7) \times 10^{-7} \text{ yr}^{-1}$ , could not exclude a fairly small value for  $\dot{P}_{orb}/P_{orb}$ . Woo et al. also noted that the inferred radius of the companion of LMC X-4,  $R \sim 8 \text{ R}_\odot$ , was significantly smaller than that of Sk 160 even though the masses are not much different, and was in the range expected for a  $\sim 15 \text{ M}_\odot$  star in the late stages of its life on the main sequence. Woo et al. concluded that the orbital decay rate of LMC X-4 was consistent with the companion star being in the late main-sequence phase.

LMC X-4 is similar in many respects to Cen X-3 and SMC X-1. It is a highly luminous X-ray source in the Large Magellanic Cloud (Giacconi et al. 1972) whose optical counterpart is a 14th magnitude OB star (Pakull 1977, Sanduleak & Philip 1977). Pulsations of the X-ray emission with a 13.5 s period demonstrate that the compact object is a neutron star (Kelley et al. 1983a). Optical photometric and spectroscopic variations which are periodic and X-rays eclipses which recur with the same period of 1.408 days revealed the binary nature and orbital period of the system (Chevalier & Illovaisky 1977, Li, Rappaport, & Epstein 1978, White 1978). A 30.5-day periodicity in the X-ray intensity, discovered by Lang et al. (1981), is most likely due to a precessing tilted accretion disk which periodically blocks our line of sight to the neutron star.

Observations of LMC X-4 which we have obtained using the *Rossi X-ray Timing Explorer (RXTE)* are described in Section 2 of this paper. Analyses and results pertaining to the timing data, a large flare, and pulse profiles are presented in Section 3. The results are discussed in Section 4.

## 2. Observations

The *RXTE* All-Sky Monitor light curve (Levine et al. 1996) of LMC X-4 was used to predict the times of the LMC X-4 30.5-d cycle high states. A 16-day interval, 1998 October 14 to 1998 October 30, was selected so as to be centered on the time of maximum intensity of one of the high states. LMC X-4 was then observed with the Proportional Counter Array (PCA; Jahoda et al. 1996) and High-Energy X-ray Timing Experiment (HEXTE) on *RXTE* during 47 intervals within this 16-day time interval. All five Proportional Counter Units (PCUs) were operating during the great majority of the observations, although a few observations were carried out with only 3 or 4 operational PCUs.

The results presented here were obtained from our analysis of the PCA data. These data were telemetered in “Goodxenon1” and “Goodxenon2” modes which preserve the 1 microsecond time resolution and the inherent energy resolution of the detectors.

The average count rate attributed to LMC X-4 for each observation outside of eclipse is shown in Figure 1 for each of two energy bands. The source intensity varied over the 16 day time interval in a manner more or less consistent with the general pattern of the 30.5 d cycle. The detected counting rates reached peak values of  $\sim 100$  and  $\sim 180$  counts  $\text{s}^{-1}$  in the 2 - 8 and 8 - 20 keV energy bands, respectively, near the expected time of maximum intensity. We note that the similarity of the variation in the two energy bands indicates that the variation cannot be attributed solely to photoelectric absorption by neutral matter of cosmic element abundances.

We estimated the X-ray luminosity of LMC X-4 by integrating the observed spectrum corrected for background and for absorption at low energies over the 2 - 25 keV energy range. The result for the average spectrum obtained from the observations of 1998 October 21 (Julian Date 2451107.85; *RXTE* observation no. 30085-01-15-00) is  $L \sim 2.3 \times 10^{38}$  ergs  $\text{s}^{-1}$  for an assumed distance of 50 kpc.

## 3. Analysis and Results

### 3.1. Timing Analysis

Pulse timing analyses have been performed with non-background-subtracted data. The “Goodxenon” events were binned into 1/16 s time bins for two energy bands, 2 - 8 keV and 8 - 20 keV. Only events

from the front xenon-filled layer of each PCU (i.e., L1 and R1) were used for the 2 - 8 keV band, while events from all three xenon-filled layers were used for the 8 - 20 keV band.

For the pulse-timing analysis, the time of each bin of data was corrected for the time delay incurred by the observation of the pulsations from LMC X-4 at the spacecraft position rather than at the barycenter of the solar system. In making these corrections we used the coordinates of LMC X-4 measured by Bradt, Doxsey, & Jernigan (1979) converted to the equinox J2000.0 reference frame, viz.,  $\alpha_{J2000} = 5^h 32^m 49.2^s$ ,  $\delta_{J2000} = -66^\circ 22' 15''$ . The times were then further corrected for the orbital motion of the pulsar according to a provisional orbital ephemeris for LMC X-4. This yields times that would have been recorded by an instrument moving with an approximately constant velocity relative to the pulsar. The corrected times were then used to fold subsets of the data according to a provisional pulsar rotation frequency and frequency derivatives up to second order.

The count rate data from each of the 47 observations were folded to produce pulse profiles. Data taken while the source was in eclipse or when a strong flare was occurring were not included in the profiles. Smearing of these profiles due to inaccuracies in the provisional parameters was less than 0.1 pulse periods.

A pulse template (see Figure 2) was constructed by averaging the profiles from 12 of the observations (interval A in Figure 3). The template was then cross correlated with the individual profiles, and a precise value for the phase corresponding to the peak of the cross correlation function was obtained via quadratic interpolation of the bin with the peak value and the nearest neighbor bins. We neglected corrections for the zero-delay autocorrelation peak that should be present in the cross correlation of the template with any of the 12 profiles used to form the template, since we believe that such corrections are presently unimportant.

The phases of the cross correlation function peaks should be regarded as differences from the phases of the pulsations of a model pulsar in a model orbit. Phase differences can result from differences between the actual orbit and the model orbit; such phase differences can properly be regarded (after being multiplied by the pulse period) as pulse arrival time differences. Phase differences which result when the spin frequency of the actual pulsar differs from that of the

model pulsar can properly be regarded as pulsar rotation phase differences. There can also be other causes of phase differences, such as changes in the intrinsic beam pattern of the pulsar or simply statistical fluctuations in the observed count rates.

We performed the pulse timing analysis on the data from each energy band separately. The cross correlation phase differences with respect to a best-fit model described below are shown in Figure 3. This figure clearly shows that phase differences which are small in magnitude, i.e.,  $< 0.1$  cycles, and relatively constant from one observation to the next were obtained for a majority but not for all of the observations. The large scatter of the phase differences for the first five observations, which were obtained when the overall source intensity was low, cannot be entirely attributed to lack of sufficient signal. Rather, the pulse profile was significantly different from the template profile during three of the five observations, while the pulsations were very weak during two of the observations.

The phase differences obtained from the last  $\sim 3$  days of the observations are not consistent between the results for the two energy bands and also show both significant changes (relative to our best fit model) as well as sudden jumps. These problems are mostly caused by substantial changes in the pulse profile which are apparent by direct inspection and by examination of the relative strengths of the harmonics of the pulse frequency in Fourier transforms. The pulse profile changes are discussed further in Section 3.3.

We fit the results for 28 observation intervals in which the phase differences appeared to be well-behaved (solid black circles in Figure 3) with a general circular orbit model to obtain corrections to the provisional orbital and pulse period ephemerides. The model included parameters for the epoch of orbital phase zero  $T_{\pi/2}$  and projected orbital radius  $a_x \sin i$  as well as parameters for the pulse epoch, frequency, and two frequency derivatives. Corrections to model parameters were obtained using a linearized (with respect to a provisional model) unweighted least-squares fitting procedure. The root mean square deviation of the observed arrival times from the model arrival times was used as an estimate of the observational uncertainty in each arrival time. The latter uncertainties were then propagated through the linear least-squares procedure to estimate  $1\sigma$  errors in the orbital and spin frequency parameters. The folding and fitting procedures were iterated using corrected

parameters until the corrections became small in comparison with their estimated uncertainties.

The parameters for the best fit circular orbit model are given in Table 1. We derive a value for  $a_x \sin i$  of  $26.34 \pm 0.02$  lt-s which is consistent with the value of  $26.31 \pm 0.07$  lt-s derived from *Ginga* observations by Levine et al. (1991). The weighted average of the fitted values of the epoch of orbital phase zero for the two energy bands is  $T_{\pi/2} = \text{JD } 2,451,111.86579 \pm 0.00010$  (TT). The estimated error in  $T_{\pi/2}$  is calculated assuming statistical independence of the errors in the results from each energy band. These errors are, in turn, estimated on the basis of the scatter of the observed arrival times relative to the model arrival times as described above. However, the difference between the values of  $T_{\pi/2}$  obtained for the two energy bands indicates that the magnitude of the error of the weighted average may be underestimated by a factor as large as  $\sim 2$ , and we therefore use an error estimate of  $0.00020$  d in our determination of the orbital decay (see below). In any case, this result is significantly more accurate than previous determinations of the epoch of phase zero of LMC X-4.

We have also fit the pulse timing results from the 28 observations with a model that allows a small eccentricity  $e$  by including parameters that are proportional to  $e \sin \Omega$  and  $e \cos \Omega$  as coefficients of  $\cos 2\omega_{\text{orb}} t$  and  $\sin 2\omega_{\text{orb}} t$ , respectively. Here,  $\Omega$  is the longitude of periastron and  $\omega_{\text{orb}}$  is the orbital angular frequency. No significant eccentricity was found, so that we report an upper limit  $e < 0.003$  ( $2\sigma$ ).

The resultant Doppler delay data, with the delays due to the best-fit circular orbit added back in, are plotted in Figure 4.

Our determination of the epoch of orbital phase zero is shown together with previously determined epochs of orbital phase zero for LMC X-4 in Figure 5. The solid curve is the best-fit quadratic function of time (see Table 1). The coefficient of the quadratic term of the fitting function implies  $\dot{P}_{\text{orb}}/P_{\text{orb}} = (-9.8 \pm 0.7) \times 10^{-7} \text{ yr}^{-1}$ . This represents the first highly significant evidence for orbital decay in LMC X-4. It is consistent with the estimate of Woo et al. (1996) who obtained  $\dot{P}_{\text{orb}}/P_{\text{orb}} = (-5.3 \pm 2.7) \times 10^{-7} \text{ yr}^{-1}$ . The coefficients for the best fit quadratic function that gives the time of the Nth eclipse in LMC X-4 may be found in Table 1.

We obtain a value for the pulse period (Table 1) which is barely shorter than that measured in

1991 with *Rosat* ( $13.50292 \pm 0.00002$  s; Woo et al. 1996). The average value of the pulse period derivative over the intervening  $\sim 7$  years is  $\dot{P}_{pulse}/P_{pulse} = (-4.9 \pm 0.2) \times 10^{-6} \text{ yr}^{-1}$  which is much smaller in magnitude than the derivative which we estimate from our timing analysis of the *RXTE* observations, i.e.,  $\dot{P}_{pulse}/P_{pulse} = (-2.14 \pm 0.02) \times 10^{-3} \text{ yr}^{-1}$ . A graph of the history of the pulse period in Woo et al. (1996) shows that episodes of both spin up and spin down have occurred during the last 20 years. Since the long-term average spin up (or spin down) rate of LMC X-4 is much smaller in magnitude than the rate typically measured during an observation of a few weeks or less in duration, the pulsar may be near its equilibrium rotation period (see also Woo et al. 1996).

### 3.2. Large Flares

It is believed that the X-ray luminosity of LMC X-4 is usually fairly constant at a value somewhat higher than the Eddington luminosity for a  $1.4 M_{\odot}$  neutron star, even though the X-ray flux observed at Earth is modulated with a 30.5-day period (Lang et al. 1981). It has been known for a long time, however, that LMC X-4 exhibits large X-ray flares, which typically last for  $\sim 1000$  sec and which occur non-periodically approximately every few days (Kelley et al. 1983a, Levine et al. 1991 and references therein). During the flares, the X-ray luminosity increases by factors of  $\sim 2$  to  $5$ , and the X-ray spectrum softens considerably.

Flares were apparent during the *RXTE* observations of 1998 October 14 (Julian Date  $\simeq 2451100.9$ , *RXTE* observation no. 30085-02-01-00), October 26 ( $\simeq 2451112.9$ , 30085-01-27-02), and October 28 ( $\simeq 2451114.1$ , 30085-01-29-00). A plot of the countrate during a portion of the largest of these flares (that of 1998 October 28) is shown in Figure 6. The observations were interrupted just after a peak in the flare by an Earth occultation of the source as seen from the moving *RXTE* spacecraft. The top panels of Figure 6 show the count rate of LMC X-4 in 2-sec time bins for the 8-20 keV and 2-8 keV energy bands. Three temporal structures are evident in the raw counting rate: the 13.5-sec pulsations, a modulation with a characteristic timescale of  $\sim 150$  sec, and an overall outburst time of  $> 400$  sec. The bottom panel of Figure 6 shows the ratio of the count rate in the 2-8 keV to that in the 8-20 keV energy channel, i.e., a “softness” ratio. As was found in previous observations of these flares, they are spectrally very

soft. Note also that the pulsations essentially disappear in the softness plot, indicating that the softness is a monotonically increasing function of the source luminosity and is not a function of pulse phase.

The peaks of the X-ray counting rates during this particular flare are up, compared with the quiescent level, by factors of 4 and 7 in the 8-20 keV and 2-8 keV bands, respectively. After properly integrating over the 2-25 keV X-ray band and averaging over at least one pulse cycle, we find that the X-ray luminosity increased by a factor of  $\sim 3$ , which yields an absolute value for the peak luminosity of the flare of  $\sim 6 \times 10^{38}$  ergs  $\text{s}^{-1}$ .

We discuss physical implications of the large X-ray flares in section 4.2.

### 3.3. Pulse Profiles

We used the best-fit orbital and pulse frequency parameters to produce three sets of pulse profiles for each of 10 energy intervals (Figures 7-9). The profile sets are averages for (1) the same 12 observations used to form the template pulse profile (interval A of Fig. 3), (2) the portion of the observation of 1998 October 28 during which a strong flare was observed (interval B), and (3) three of the later observations (interval C) in which the 8 - 20 keV pulse phase was quite different from that anticipated from the 28 observations used for the pulse timing fits.

The profiles in Figure 7 can be compared with the non-flare profiles obtained from *Ginga* observations in 1988 (shown in Woo et al. 1996) and 1989 (shown in Levine et al. 1991). As a rough approximation, the profiles can be thought of as consisting of an underlying sinusoid with phase and strength that may vary with photon energy and a prominent pair of narrow absorption dips. In both the *Ginga* and *RXTE* sets of non-flare profiles the narrow dips (at phases  $\sim 0.58$  and  $0.82$  in Figure 7) are separated by  $\Delta\phi \sim 0.25$  and the first dip is more prominent, i.e., deeper, than the second. In general, the dips exhibit structure on time scales down to the time resolution of the folded profiles, e.g.,  $\sim 0.27$  s in Figure 7. In the *Ginga* profiles the underlying sinusoidal profile appears to be stronger at low energies and shifted in phase (relative to the dips) in comparison with the underlying sinusoid in the present *RXTE* profiles.

Average pulse profiles during the time of the strong flare are shown in Figure 8. The definition of pulse phase zero is the same as for the profiles shown in

Figures 7 and 9. In general, the pulse profiles during the flare are simpler than those outside of the flare and are essentially sinusoidal at all energies studied. Moreover, during the flare the pulses are in phase at all energies, in contrast with the profiles outside of the flares. We also note that the flare profiles are very similar to the flare pulse profiles obtained from *Ginga* observations in 1989 (see Levine et al. 1991).

The set of pulse profiles produced from data taken late in the *RXTE* observation of LMC X-4, and during an interval when there was no obvious flaring activity, is shown in Figure 9. These profiles are very similar to those obtained during the flare (see Figure 8) in that they are rather sinusoidal in shape, and in phase at all energies. However, the fractional amplitude of the modulation is much lower in the profiles in Fig. 9 than in the flare profiles. This is a dramatic example of how the pulse profiles can change long ( $\sim$  a day) after the occurrence of a major flare, although it is possible that strong flares may have occurred closer to these later observations during the large gaps in observational coverage. It is changes in pulse shape such as these that account for the occasional erratic behavior of the pulse phase, as exhibited in Figure 3.

## 4. Discussion

### 4.1. Orbital Period Changes

Levine et al. (1993) discuss orbital period changes in the context of the measured orbital period derivative of SMC X-1. They derive an estimate for the orbital period derivative for the situation where expansion of the companion star drives the orbital decay. Their discussion is pertinent when the logarithmic expansion rate of the companion is roughly constant for at least the time necessary to establish a pseudo-equilibrium in the difference between the rotation frequency of the companion star and the orbital frequency. In this case the orbital period derivative is given by (eqn. 6 of Levine et al. 1993)

$$\frac{\dot{P}_{orb}}{P_{orb}} \simeq -\frac{\omega_c d \ln(I)/dt}{\omega_K(\mu a^2/3I - 1)} \quad (1)$$

where  $\omega_c$  and  $\omega_K$  are, respectively, the angular frequencies of the companion's rotation and the orbital motion,  $I$  is the moment of inertia of the companion,  $\mu$  is the system reduced mass, and  $a$  is the separation of the centers of the two stars.

Monte Carlo analysis of the binary system parameters of LMC X-4 yields an estimated mass of the

companion of 12 to  $18 M_{\odot}$  (see Joss & Rappaport 1984, Nagase 1989, Levine et al. 1991). Stellar evolution calculations for a  $15 M_{\odot}$  star (Ph. Podsiadlowski 1991, private communication) show that the rate of increase of the companion star's moment of inertia can be as large as  $d \ln(I)/dt \sim 3 \times 10^{-7} \text{ yr}^{-1}$  near the end of the main-sequence phase when the supply of hydrogen in the star's core is nearly exhausted. The Monte Carlo analysis of the system parameters also indicates that the factor  $(\mu a^2/3I - 1)$  most likely has a value in the range of 0.3 to 1.1. This would then yield an orbital period derivative  $\dot{P}_{orb}/P_{orb} \sim -(3 - 10) \times 10^{-7} \text{ yr}^{-1}$  which is compatible with the measured value  $\dot{P}_{orb}/P_{orb} = (-9.8 \pm 0.7) \times 10^{-7} \text{ yr}^{-1}$ .

The radius of the companion star is estimated from the Monte Carlo analysis to be in the range  $6 - 9 R_{\odot}$  (Joss & Rappaport 1984, Nagase 1989, Levine et al. 1991) which is compatible with the radius near the end of the main-sequence phase derived by Podsiadlowski.

One problem is that the optically-observed luminosity and temperature place the companion in a region of the H-R diagram which indicates a mass of  $\sim 25 M_{\odot}$ . We note that the calculations of Podsiadlowski did not incorporate several effects which could be important in this regard, e.g., mass loss via a wind, effects of the evolution of the companion in a binary system with the likelihood that substantial mass transfer has occurred, the low metallicity of stars in the LMC, effects of X-ray illumination, etc.

### 4.2. Large X-Ray Flares

The three large flares seen in the present observations are similar in all respects to the flares of LMC X-4 observed in detail on earlier occasions (Levine et al. 1991 and references therein). During such flares the X-ray luminosity (2-25 keV) goes from its typical nearly steady value of  $\sim 2 \times 10^{38} \text{ ergs s}^{-1}$  up to  $\sim 10^{39} \text{ ergs s}^{-1}$ , and the modulation factor of the pulsations increases substantially. As the luminosity (computed using the flux averaged over a pulse cycle) increases by factors of 2 to 5, the X-ray spectrum softens considerably. While the X-ray spectrum during neither the flaring nor quiescent modes is well fit by a black-body, we can say that the characteristic temperature associated with the emission decreases by about a factor of 2 during the flaring state. This was shown for the instance of the flare observed on 1998 October 28 by fitting the spectrum with the exponential form  $e^{-E/kT}$ . The total energy released in a flare is typi-

cally  $\sim 10^{41}$  ergs. Finally, we point out that no other known accretion-powered X-ray pulsar exhibits such flares.

From the perspective of a simple thermalization scenario, a factor of 2 to 5 increase in luminosity, coupled with a decrease in temperature by a factor of  $\sim 2$ , leads us to infer that the emitting area increases by a factor of about 50!. For a nominal polar cap surface area of  $\sim 3 \text{ km}^2$ , which might correspond to the accreting area during the quiescent state, the emitting area during the flare would have to increase to more than  $\sim 100 \text{ km}^2$ . This is equivalent to the surface area of a cylindrical accretion column 25 km tall with a diameter of 2 km or of a polar cap that is 15 km in diameter.

The obvious question that arises is “what is the physical origin of the large flaring events?” We discuss briefly three possible origins for the flares: (1) an instability which dumps  $\sim 10^{21}$  grams of matter stored in the accretion disk or magnetosphere, with the attendant release of gravitational potential energy; (2) the release of nuclear energy due to the fusion of carbon or heavier elements below the surface of the neutron star; and (3) an event involving the release of magnetic energy.

It is commonly thought that variations in accretion rate are responsible for the ubiquitous variability and the flaring commonly seen in a large fraction of X-ray binaries. Accretion events must therefore be considered as candidate sources of energy for the LMC X-4 flares. On the other hand, the flaring in LMC X-4 is quite distinct from the variability and flaring in other X-ray binaries, including the Type II X-ray bursts that are attributed to accretion instabilities in the Rapid Burster (MXB 1730-335) and GRO J1744-28 (Guerriero et al. 1999, Nishiuchi et al. 1999, Woods et al. 1999 and references therein). Moreover, in a high-strength magnetic field pulsar such as LMC X-4, the inferred increase in surface area during the flares does not seem to have a ready physical interpretation. For example, emission from the sides of an accretion column might require a height of more than a neutron star radius. In order to confidently retain the picture of the flares as accretion events, one would like to be able to model accretion onto the polar caps of a neutron star at the Eddington limit, increase the rate by a factor of  $\sim 5$  for  $\sim 1000$  sec, and compute the expected spectrum at least well enough to demonstrate the observed softening. To our knowledge, this has not been done.

An energy release of  $\sim 10^{41}$  ergs, within the context of a nuclear burning scenario (Brown & Bildsten 1998) would require burning  $\sim 10^{23}$  g of carbon or heavier elements, with a nuclear burning efficiency of  $\sim 10^{-3}$ . (Hydrogen and helium are burned almost as quickly as they are accreted very near the surface of the neutron star.) This scenario has the advantage that if the nuclear burning takes place over a region of the neutron star surface that is larger than the footprint of the accretion flow, the flare spectrum would naturally be expected to be softer than the quiescent spectrum. At accretion rates of  $10^{18} \text{ g s}^{-1}$ , the mean time between outbursts would be  $\sim 10^5$  s ( $\sim 1$  day), which is roughly typical of flare recurrence times. The large and fairly constant  $\sim 50\%$  modulation factor of the pulses during the flares, compared with only  $\sim 20\%$  away from the flares, might be explained by subsurface nuclear burning that takes place at only one of the two magnetic poles during a particular event, so that substantial modulation would be observed as the polar cap rotates in and out of view. However, the subflare structure observed on a timescale of  $\sim 150$  s lacks a natural explanation in the context of a deep nuclear burning scenario. Finally, in this regard we note that Brown & Bildsten (1998) found difficulties explaining the large flares in LMC X-4 with carbon burning. The principal difficulty is the fact that accretion of H-rich material is thought to produce much heavier “ashes” than carbon, in which case not much carbon would be expected to accumulate and be available to power the flares.

Finally, we consider the possibility that magnetic energy powers the flares. Magnetic energy might be suddenly released, e.g., if the accreting material at the polar caps were somehow able to compress the magnetic field until an instability leads to a reconnection of the field lines. The energy of  $\sim 10^{41}$  ergs in a flare would require that the product of magnetic field and volume be

$$B_{13}^2 V_{\text{km}^3} \simeq 25 \quad (2)$$

where  $B_{13}$  is the surface magnetic field strength in units of  $10^{13}$  G, and  $V_{\text{km}^3}$  is the volume in units of cubic kilometers. For  $B_{13} = 1$ , the magnetic energy of  $\sim 1\%$  of the neutron star volume or, alternatively, of its magnetosphere would need to be released. If this is true, then the field would need to be regenerated, since observations suggest that flares have occurred every few days over the past 20 years, at least. To our knowledge, the detailed physics of such a scenario

has not yet been explored.

We also suggest the possibility of a connection between LMC X-4 and soft gamma repeaters (Kouveliotou 1999) within the context of the magnetar model (Thompson & Duncan 1995). If the neutron star in LMC X-4 is rotating at about the equilibrium rate estimated in the standard accretion torque model (Lamb, Pethick, & Pines 1973, Rappaport & Joss 1977, Ghosh & Lamb 1979, Bildsten et al. 1997), this could imply a surface dipole field strength of  $\sim 3 \times 10^{13}$  G. This is stronger than the canonical  $10^{12}$  G field strength thought to be typical of accretion-powered pulsars, but is somewhat below the field strengths thought to characterize magnetars. Perhaps the facts that the LMC X-4 flares are longer in duration and have softer spectra than the bursts of soft-gamma repeaters is related to a lower magnetic field strength and the presence of accretion in LMC X-4.

Thus, at this point, we are uncertain as to whether the origin of the energy in the flares is gravitational, nuclear, or magnetic. However, LMC X-4 is unique in its flaring behavior, and the resolution of the origin of the flares may well provide a key to understanding some fundamental property of the neutron star.

The authors gratefully acknowledge useful conversations with Lars Bildsten, Andrei Gruzinov, Ed Morgan, Mike Muno, and Henk Spruit. We also thank Mike Muno for assistance with the spectral analysis. This work was supported in part by NASA Grant NAG5-8244 and by NASA Contract NAS5-30612.

## REFERENCES

Bradt, H. V., Doxsey, R. E., & Jernigan, J. G. 1979, in *X-ray Astronomy*, ed. W. A. Baity & L. E. Peterson, p. 3, (Oxford:Pergamon)

Bildsten, L., et al. 1997, ApJS, 113, 367, astro-ph/9707125

Brown, E. F., & Bildsten, L. 1998, ApJ, 496, 915, astro-ph/9710261

Chevalier, C., & Ilovaisky, S. A. 1977, A&A, 59, L9

Corbet, R. H. D., Woo, J. W., & Nagase, F. 1993, A&A, 276, 52

Deeter, J. E., Boynton, P. E., Miyamoto, S., Kitamoto, S., Nagase, F., & Kawai, N. 1991, ApJ, 383, 324

Dennerl, K. 1991, Thesis - Ludwig-Maximilians Univ. Max-Planck-Inst. für Physik und Astrophysik, Garching (Germany)

Ghosh, P., & Lamb, F. K. 1979, ApJ, 234, 296

Giacconi, R., Murray, S., Gursky, H., Kellogg, E., Schreier, E., & Tananbaum, H. 1972, ApJ, 178, 281

Guerriero, R., et al. 1999, MNRAS, 307, 179, astro-ph/9807110

Kelley, R. L., Jernigan, J. G., Levine, A., Petro, L. D., & Rappaport, S. 1983a, ApJ, 264, 568

Kelley, R. L., Rappaport, S., Clark, G. W., & Petro, L. D. 1983b, ApJ, 268, 790

Kelley, R. L. 1986, in *The Evolution of Galactic X-ray Sources*, ed. J. Truemper et al. (Dordrecht:Reidel), 75

Kitamoto, S., et al. 1995, PASJ, 47, 233

Kouveliotou, C. 1999, Proc. Natl. Acad. Sci., 96, 5351

Jahoda, K., Swank, J. H., Giles, A. B., Stark, M. J., Strohmayer, T., Zhang, W., & Morgan, E. 1996, Proc. SPIE, 2808, 59

Joss, P. C., & Rappaport, S. 1984, ARA&A, 22, 537

Lamb, F. K., Pethick, C. J., & Pines, D. 1973, ApJ, 184, 271

Lang, F. L., et al. 1981, ApJ, 246, L21

Levine, A. M., Bradt, H., Cui, W., Jernigan, J. G., Morgan, E. H., Remillard, R., Shirey, R. E., & Smith, D. A. 1996, ApJ, 469, L33, astro-ph/9608109

Levine, A., Rappaport, S., Deeter, J. E., Boynton, P. E., & Nagase, F. 1993, ApJ, 410, 328

Levine, A., Rappaport, S., Putney, A., Corbet, R., & Nagase, F. 1991, ApJ, 381, 101

Li, F., Rappaport, S., & Epstein, A. 1978, Nature, 271, 37

Nagase, F. 1989, PASJ, 41, 1

Nishiuchi, M., et al. 1999, ApJ, 517, 436, astro-ph/9812298

TABLE 1  
ORBITAL AND PULSE PARAMETERS FOR LMC X-4

| Parameter                         | Value <sup>a</sup> (2-8 keV)                    | Value <sup>a</sup> (8-20 keV)                  |
|-----------------------------------|---|--|
| $a_x \sin i$ <sup>b</sup>         | $26.333 \pm 0.019$ lt-s                         | $26.370 \pm 0.031$ lt-s                        |
| $e$                               | $< 0.003$ ( $2\sigma$ )                         |  |
| $T_{\pi/2}$ <sup>c</sup>          | MJD <sup>d</sup> $51110.86571 \pm 0.00012$ (TT) | MJD $51110.86600 \pm 0.00020$ (TT)             |
| $\nu_{pulse}$ <sup>e,f</sup>      | $0.074060687 \pm 0.000000010$ Hz                | $0.074060697 \pm 0.000000016$ Hz               |
| $\dot{\nu}_{pulse}$ <sup>e</sup>  | $(5.01 \pm 0.04) \times 10^{-12}$ Hz s $^{-1}$  | $(5.11 \pm 0.07) \times 10^{-12}$ Hz s $^{-1}$ |
| $\ddot{\nu}_{pulse}$ <sup>e</sup> | $(-1.4 \pm 0.7) \times 10^{-18}$ Hz s $^{-2}$   | $(-1.2 \pm 1.2) \times 10^{-18}$ Hz s $^{-2}$  |
| $a_0$ <sup>g</sup>                | JD 2,448,138.2500 $\pm 0.0004$ (TT)             |  |
| $a_1$ <sup>g</sup>                | $1.40839776 \pm 0.00000026$ days                |  |
| $a_2$ <sup>g</sup>                | $(-2.65 \pm 0.19) \times 10^{-9}$ days          |  |
| $\dot{P}_{orb}/P_{orb}$           | $(-9.8 \pm 0.7) \times 10^{-7}$ yr $^{-1}$      |  |

<sup>a</sup>The errors ( $1\sigma$ ) have been obtained from a least-squares analysis in which the  $1\sigma$  errors of the observed pulse arrival times were estimated by the root mean square deviation of the measurements from the best fit model. This may underestimate the effects of certain types of systematic errors.

<sup>b</sup> $a_x \sin i$  weighted average =  $26.343 \pm 0.016$  lt-s

<sup>c</sup> $T_{\pi/2}$  average = MJD  $51110.86579 \pm 0.00010$  (TT) (but see text)

<sup>d</sup>Modified Julian Date = Julian Date – 2,400,000.5

<sup>e</sup>For the epoch MJD 51235.0

<sup>f</sup> $P_{pulse} = 13.502440 \pm 0.000002$  s (2-8 keV) or  $13.502439 \pm 0.000003$  s (8-20 keV)

<sup>g</sup>The time of the  $N$ th eclipse can be written as:  $t_N = a_0 + a_1 N + a_2 N^2$ .

Pakull, M. W. 1977, IAU Circ., No. 3017

Rappaport, S., & Joss, P. C. 1977, Nature, 266, 683

Safi-Harb, S., Ögelman, H., & Dennerl, K. 1996, ApJ, 456, L37

Sanduleak, N., & Philip, A. G. D. 1977, IAU Circ., No. 3023

Thompson, C., & Duncan, R. C. 1995, MNRAS, 275, 255

van Kerkwijk, M. H., Geballe, T. R., King, D. L., van der Klis, M., & van Paradijs, J. 1996, A&A, 314, 521, astro-ph/9604100

White, N. E. 1978, Nature, 271, 38

Woo, J. W., Clark, G. W., Levine, A. M., Corbet, R. H. D., & Nagase, F. 1996, ApJ, 467, 811

Woods, P. M., et al. 1999, ApJ, 517, 431

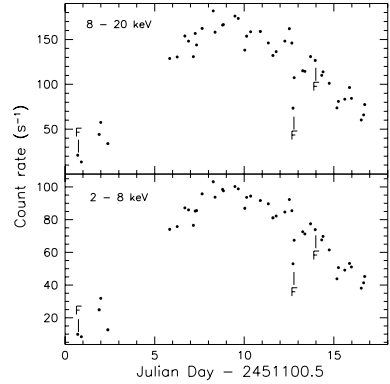


Fig. 1.— Average background-subtracted count rates in 2 energy bands for 46 of the 47 observations of LMC X-4 obtained in 1998 October with the PCA on *RXTE*. Time intervals during an eclipse or during a flare event have been excluded for purposes of computing the average rates. Observations in which strong flares were observed are denoted by an “F”. In the few instances when fewer than 5 PCUs were in operation, the rates have been normalized to a 5 PCU basis. Julian Date 2,451,100.5 corresponds to 1998 October 14 0<sup>h</sup> TT.

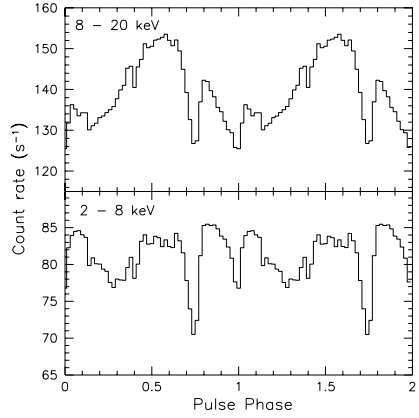


Fig. 2.— Average pulse profiles for 2 energy bands for 12 observations of LMC X-4 (see interval A in Fig. 3). These profiles were used as the templates for our pulse timing analysis. The 1 $\sigma$  uncertainties from counting statistics are approximately 0.5 counts s<sup>-1</sup>.

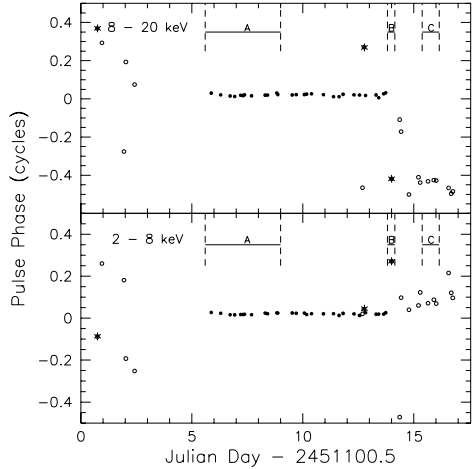


Fig. 3.— Results of our pulse timing analysis for 2 energy bands. Each symbol gives the phase of the pulse profile for one of the 47 observations of LMC X-4 relative to the phase of a model pulsar. The solid circles indicate measurements that we use in the least-squares fit to obtain orbital and spin parameters. The open circles are measurements that are not used in the fit because the timing results here indicate significant inconsistencies from the results expected from a pulsar with an invariant pulse profile. The observations in which strong flares occurred are denoted by “\*”; however, the data taken during the flares were not included in the pulse profiles made for the timing analysis. Time interval A was used for the construction of the template pulse profiles (Fig. 2). Time intervals A, B, and C were used to make the energy-dependent profiles shown in Figures 7-9, respectively.

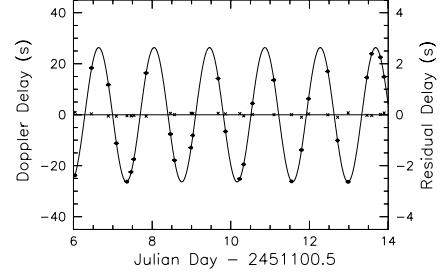


Fig. 4.— Inferred pulse arrival time delays for 28 observations of LMC X-4. The solid circles and sine wave fit show the delays with respect to a model pulsar at the center of mass of the binary system (scale on left), while the crosses show the measured time delays relative to a pulsar in the best fit orbit (scale on right).

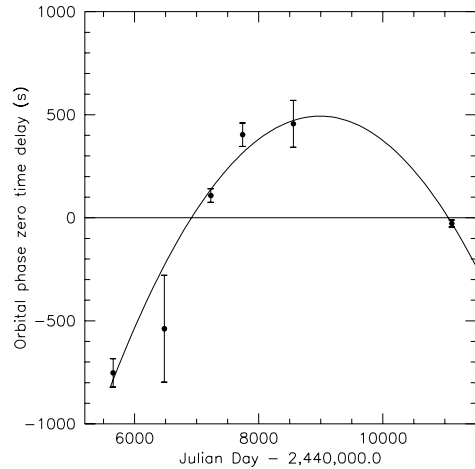


Fig. 5.— Epochs of orbital phase zero of LMC X-4 are shown relative to the epochs expected according to the best-fit constant orbital period of 1.40839457 days. The measurements are based on *EXOSAT*, *Ginga*, and *Rosat* data (Dennerl 1991; Levine et al. 1991; Woo et al. 1996) and the present work. The curve shows the best-fit quadratic function. The error bars shown indicate  $\pm 1\sigma$  uncertainties.

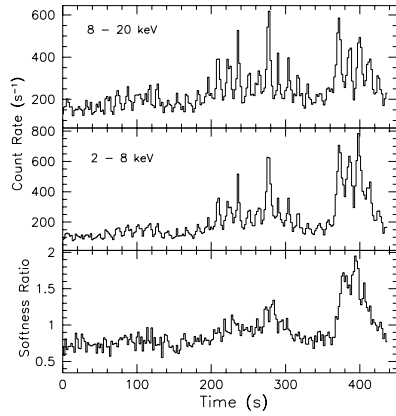


Fig. 6.— (top and middle) Background-subtracted count rates for 2 energy bands during a portion of the observation of 1998 October 28 (*RXTE* observation no. 30085-01-29-00) when a strong flare was in progress. The observation was terminated by Earth occultation of the source at about 430 s while the flare was in progress. The 13.5 s pulsations are highly evident in both energy bands. (bottom) The softness ratio defined by the number of counts in the 2–8 keV band divided by the number in the 8–20 keV band. The rates and the softness ratio are averaged in 2 s time bins. The 13.5 s pulsations are not evident in this plot.

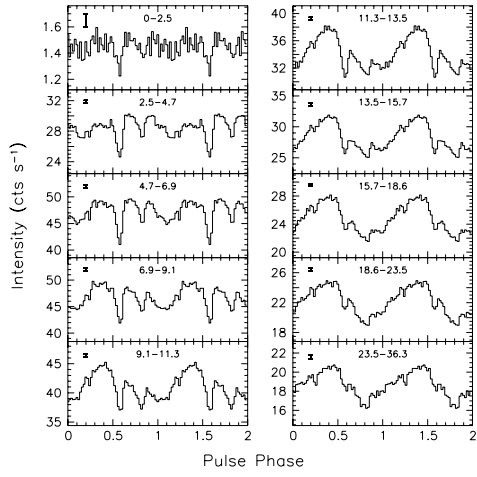


Fig. 7.— Average background-subtracted pulse profiles for 10 energy bands for the 12 observations in time interval A (see Fig. 3). Each profile is plotted twice for clarity. A typical  $\pm 1\sigma$  error and the energy range in keV are shown for each profile.

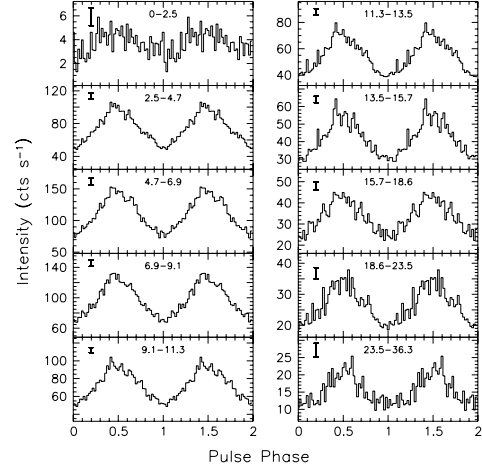


Fig. 8.— Average background-subtracted pulse profiles for 10 energy bands for the observation of the flare which occurred on 1998 October 28 (during interval B of Fig. 3). The profiles were constructed using data from the entire time interval plotted in Fig. 6. Each profile is plotted twice for clarity. A typical  $\pm 1\sigma$  error and the energy range in keV are shown for each profile.

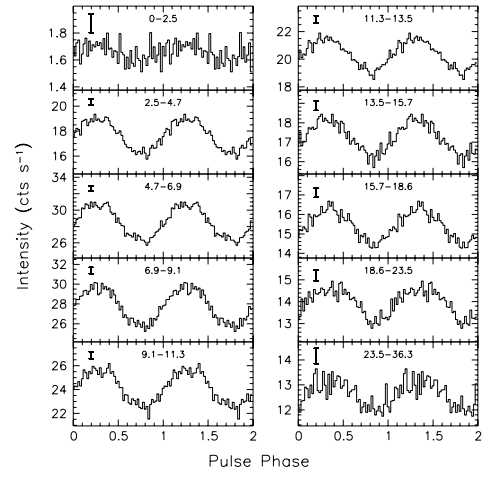


Fig. 9.— Average background-subtracted pulse profiles for 10 energy bands for the 3 observations in time interval C (see Fig. 3). Each profile is plotted twice for clarity. A typical  $\pm 1\sigma$  error and the energy range in keV are shown for each profile.